Title

Vertically integrated photo junction-field-effect transistor pixels for retinal prosthesis.

Journal

Biomedical Optics Express, 11(1)

ISSN

2156-7085

Authors

Damle, Samir

Liu, Yu-Hsin

Arya, Shaurya

et al.

Publication Date

2020

DOI

10.1364/BOE.11.000055

Peer reviewed

Research Article | Vol. 11, No. 1 / 1 January 2020 / Biomedical Optics Express 55
Biomedical Optics EXPRESS

Vertically integrated photo junction-field-effect transistor pixels for retinal prosthesis

SAMIR DAMLE,[1,*] YU-HSIN LIU,[2] SHAURYA ARYA,[3] NICHOLAS W. OESCH,[4,5] AND YU-HWA LO[5]

[1]Department of Bioengineering, University of California San Diego, 9500 Gilman Drive La Jolla, CA 92093, USA
[2]Nanovision Biosciences, Inc., 3366 N. Torrey Pines Court, Suite 220, La Jolla, CA 92037, USA
[3]Department of Electrical and Computer Engineering, University of California San Diego, Engineer Ln, La Jolla, CA 92161, USA
[4]Department of Psychology, University of California San Diego, 9500 Gilman Drive, CA 92093, USA
[5]Jacobs Retina Center at Shiley Eye Institute, Department of Ophthalmology, University of California San Diego, 9415 Campus Point Drive San Diego, CA 92093, USA
[*]sdamle@ucsd.edu

Abstract: Optoelectronic retinal prostheses transduce light into electrical current for neural stimulation. We introduce a novel optoelectronic pixel architecture consisting of a vertically integrated photo junction-field-effect transistor (Photo-JFET) and neural stimulating electrode. Experimental measurements demonstrate that optically addressed Photo-JFET pixels utilize phototransistive gain to produce a broad range of neural stimulation current and can effectively stimulate retinal neurons in vitro. The compact nature of the Photo-JFET pixel can enable high resolution retinal prostheses with the smallest reported optoelectronic pixel size to help restore high visual acuity in patients with degenerative retinal diseases.

1. Introduction

Degenerative retinal diseases including Retinitis Pigmentosa (RP) and Age-Related Macular Degeneration (AMD) are leading causes of blindness worldwide. Globally about 1 in 4000 people are affected by RP and 170 million individuals suffer from AMD [1–4]. Patients with retinal degenerative diseases suffer from the selective loss of the photoreceptive cells of the retina, while the remaining retina remains intact. Retinal implants transduce visual information into current for neural stimulation with the goal of replacing lost photoreceptor function in patients blinded by degenerative diseases. These implants, known as retinal prostheses, aim to reestablish high acuity central vision with sufficiently large visual field without compromising any residual functional areas of the retina [5].

In general, a retinal prosthesis consists of a pixelated image sensor, a stimulation encoder, an array of neural stimulation electrodes, and a power supply. One category of retinal implant utilizes a head mounted camera to capture the visual scene that is relayed by a wireless inductive link to an implanted microprocessor. The microprocessor encodes the visual scene and relays necessary neural stimulation parameters to an array of directly wired stimulation electrodes implanted in close proximity to retinal neurons [6]. A prominent example of such a retinal implant is the Argus II Retinal Prosthesis (Second Sight Medical Technologies) which has received FDA approval (2014) and CE Mark (2011) to treat Retinitis Pigmentosa patients with bare or no light perception. The best visual acuity result in Argus II patients is on the order of 20/1260 [7,8].

Another category of retinal implant utilizes a directly implanted microphotodiode array (MPDA) to convert the spatiotemporal pattern of light impinging on the MPDA into electrical currents to stimulate the retina. However, the intensity of light under typical natural retinal irradiance (0.001-1uW/mm^2) is orders of magnitude too low to be efficiently converted into

#379733 https://doi.org/10.1364/BOE.11.000055
Journal © 2020 Received 4 Oct 2019; revised 20 Nov 2019; accepted 24 Nov 2019; published 4 Dec 2019

Biomedical Optics EXPRESS

electrical current for neural stimulation (μA) by a single photodiode [9,10]. Therefore, one approach of MPDA implants is to utilize an ASIC design with a CMOS amplifier circuit within each pixel to amplify the primary photocurrent. An advantage of the CMOS ASIC approach is that the implant can encode spatiotemporal contrast across any typical visual scene without the need for externally worn imaging components [11,12]. The Alpha AMS/IMS system is an example of MPDA retinal implant with a CMOS ASIC design that has successfully received CE Mark. In clinical trials the Alpha AMS restored a best reported visual acuity nearing 20/546 [13,14]. A drawback to the CMOSASIC approach, however, is the complexity of the required hardware that limits the fill factor and requires extensive encapsulation materials to electrically insulate the array and achieve biocompatibility [15].

An alternative MPDA retinal prosthetic approach is to use photodiodes and an external light source in the NIR wavelength to power and control the current produced by the array. Pulsed near infrared light is used to optically address the implanted photodiodes with sufficient irradiance to produce photocurrent for neural stimulation. This solution can greatly simplify the form factor of the implanted hardware by using only photodiodes operated in photovoltaic mode or as actively biased pixels sharing a common power line [9,16–18]. The prosthetic visual acuity of photodiode-only arrays is on the order of 20/200- 20/400 [19]. However, a fundamental limitation of this approach is the high intensity of irradiating NIR light and the relatively large pixel area required for a photodiode to produce the necessary photocurrent to achieve neural stimulation. Stimulation of retinal neural cells requires electrical current pulses of 0.5-10 ms duration to deliver 1-100nC of charge [20]. Typical silicon photodiodes have a light conversion efficacy less than 0.8 A/W at 100% quantum efficiency. This approach thus necessitates pixel diameters on the order of 40-100 μm and 5-25 mW/mm^2 of pulsed infrared light projected onto the eye, a power level close to the maximum permissible exposure of cornea and retina [16,21,22]. Therefore, there is inherently a tradeoff between minimizing pixel size to increase prosthesis resolution and the range of photocurrent to drive neural stimulation.

To overcome these limitations, we propose a photosensitive junction-field-effect transistor (Photo-JFET) that integrates a photodetector, amplifier, and neural electrode stimulator within a single silicon pixel mesa, thus achieving gain without sacrificing fill factor. Incorporating a gain mechanism into the body of a photo sensing pixel further advances existing retinal prostheses by enabling scaling of pixel size down to 10-20 μm to achieve improved visual acuity over existing optoelectronic prostheses. In this work we describe a vertically integrated Photo-JFET device structure that can produce a broad range of current (0.1-100μA) for robust retinal neural stimulation within a safe range of NIR irradiance with the potential to restore high acuity vision for the smallest reported retinal prosthesis pixel size.

2. Design of Photo-JFET pixel architecture for retinal prosthesis

A vertically integrated Photo-JFET pixel consists of a pair of back-to-back p/n diodes in parallel with a sidewall junction-field-effect transistor (Fig. 1(A)). The diodes can be configured in either a N-P-N or P-N-P configuration for a n-channel or p-channel JFET. Here we consider only an N-P-N structure. A dielectric film is deposited on the sidewall of the silicon mesa for passivation and to induce a weak inversion layer along the vertical edge of the middle layer of the back-to-back diode, forming a vertical channel along the mesa sidewall. Silicon dioxide (SiO_2) or aluminum oxide (Al_2O_3) can be used to control the pinch-off voltage of the sidewall JFET. The sidewall oxide layer is not part of the active device but is mainly for side wall passivation. The Photo-JFET is therefore a 2-terminal device with one contact on the back of the substrate and the other contact on the top of the N-P-N mesa. A voltage bias applied across the top and bottom diodes can provide drain-source voltage (V_{DS}) for the Photo-JFET, and the same voltage also provides reverse and forward bias of two back-to-back p/n junctions. A positive voltage applied to the top contact will reverse bias the top P/N junction and forward bias the bottom P/N

Biomedical Optics EXPRESS

junction. A negative voltage applied to the top contact will forward the bias the top P/N junction and reverse bias the bottom P/N junction. The Photo-JFET is normally off in the dark and can be turned on by incident light. Here the doping profile and thickness of the vertical N-P-N structure are designed in such a way that the structure does not perform as a regular bipolar transistor (i.e. the current gain of the bipolar structure h_{fe}<<1). Instead, the structure can be modeled as 2 back-to-back P/N diodes, and the only transistor function is provided by the sidewall FET.

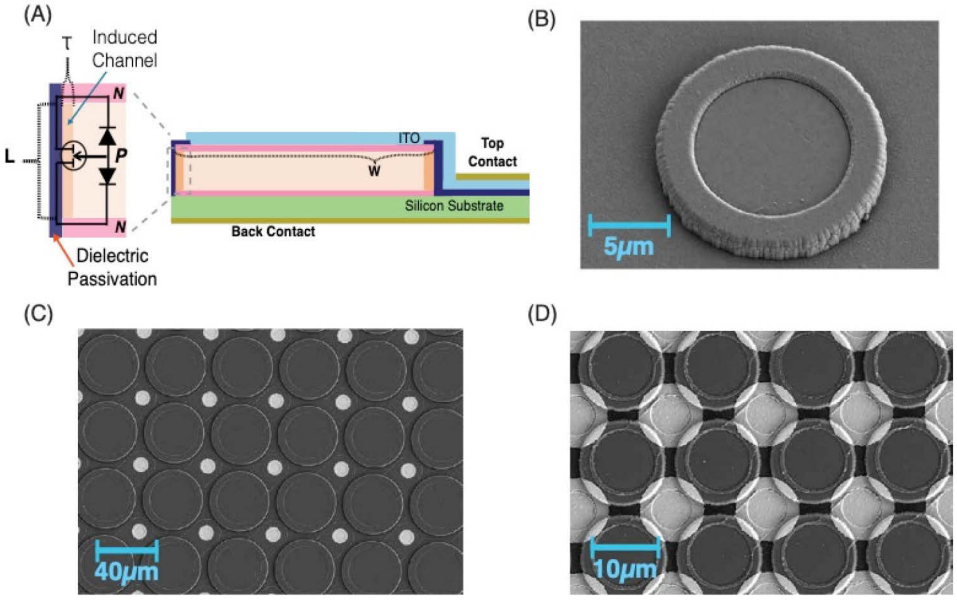

Fig. 1. (A) Design of a Photo-JFET pixel from a vertical etched mesa. A dielectric passivation layer deposited on the sidewall of the silicon mesa induces a channel along the vertical wall of the middle layer of the mesa. The sidewall view illustrates the pair of back-to-back p/n diodes and the junction-field-effect transistor (JFET) realized as an NPN or PNP stack. (B) Scanning electron microscope micrograph (SEM) of a 13 μm Photo-JFET single pixel test structure. The mesa sidewall and outer rim are coated in SiO_2 layer while electrical contact is made through a center opening in the passivation. (C) SEM micrograph of prototype array with 40 μm pixels paired with 10 μm electrodes (light gray) spaced at 45 μm pitch, a theoretical prosthetic acuity of 20/188 (D) SEM micrograph of prototype array with 13 μm pixels paired with 10 μm electrodes (light gray) spaced at 15 μm pitch

2.1. Operation principle

Under illumination the reverse biased p/n diode produces a photocurrent (I_{ph}). Both the photocurrent (I_{ph}) and the reverse saturation current (I_{o1}) flow through the forward biased p/n junction, increasing the voltage drop in the forward biased p/n junction according to the Shockley diode model:

$$V_{GS} = \eta V_T \ln\left(1 + \frac{I_{o1} + I_{ph}}{I_{o2}}\right) \tag{1}$$

where η is the ideality factor, V_T is the thermal voltage, and I_{o2} is the reverse saturation current for the forward biased p/n junction. Note that in our design, V_{GS} in Eq. (1) is the voltage drop across the forward-biased p/n junction, which can also be considered the gate-to-source bias for the mesa sidewall FET. At sufficient voltage, the gate-to-source bias (V_{GS}) induces a conductive n-channel along the sidewall of the p-layer, turning on the FET. In an ideal design, the threshold

Biomedical Optics EXPRESS

voltage required (V_{THmin}) to turn on the normally-off JFET will be greater than the V_{GS} produced by dark current (I_{o1}) but low enough such that the channel will turn on at low irradiance (Eq. (2) for a N-channel JFET). The actual threshold voltage of the JFET depends on the doping of the middle p-doped region for the N-P-N configuration and the dielectric-silicon mesa interface. Importantly for a retinal prosthesis, a Photo-JFET can be engineered with high V_{TH} and operated by optical addressing with NIR irradiance to control contrast and adjust the range of available photocurrent to the correct range for neural stimulation. Figure 2(A) demonstrates the range of possible V_{GS} calculated for lighting conditions spanning a range from retinal irradiance under dim lighting conditions to the typical irradiance of supplemental NIR light used in retinal prostheses as described above.

$$V_{TH\,\min} > \eta V_T \ln\left(1 + \frac{I_{o1}}{I_{o2}}\right) \tag{2}$$

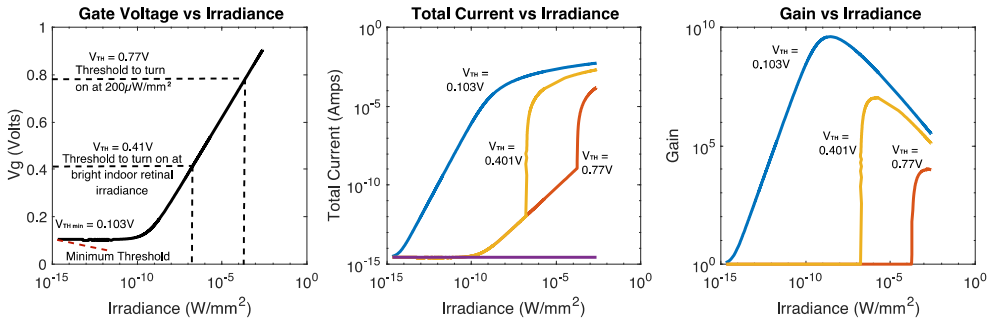

Fig. 2. Theoretical performance characteristics of a vertical silicon Photo-JFET using typical device parameters for a range of retinal irradiance. (a) Calculated gate to source voltage (V_{GS}) for a range of irradiance conditions following Eq. (1). Marked on the graph are the possible values of the threshold voltage to turn on the JFET channel for ideal case of minimum threshold, bright indoor retinal irradiance, and 200μW/mm^2 supplemented NIR. (b) Calculated total current (I_{Tot}) using the identified threshold voltages in (a). (c) Calculated gain achieved over the irradiance range. For simplicity, we have ignored the subthreshold current in (b) and (c), thus underestimating the total current and gain in subthreshold regime.

2.2. Photocurrent amplification

With sufficient illumination the V_{GS} will exceed the threshold voltage (V_{TH}) to turn on the JFET and modulate the drain current (I_D) across the channel. The drain current in the saturation region for a normally-off N-channel JFET can be represented by Eq. (3) where W is the effective channel width, equal to the circumference of the mesa, L is the length of the vertical channel, a is the effective channel width controlled by the thickness of charge inversion layer at the oxide-silicon mesa sidewall interface. The net output current in response to the input light is the sum of the original primary photocurrent across the back-to-back p/n junctions (I_{ph}) and the drain current (I_D) through the sidewall JFET.

$$I_D = \frac{W\mu\varepsilon s}{2La}(V_{GS} - V_{TH})^2 \tag{3}$$

Combining Eqs. (1) and (3) and under the condition that the photocurrent is much greater than the reverse saturation current I_{o1}, we obtain the drain current of the sidewall JFET represented by

Biomedical Optics EXPRESS

Eq. (4) when the JFET is in saturation region.

$$I_D = \frac{W\mu\varepsilon s}{2La}\left[\eta V_T \ln\left(1 + \frac{I_{ph}}{I_{o2}}\right) - V_{TH}\right]^2 \tag{4}$$

The total current produced by a Photo-JFET pixel under illumination is the sum of the drain current and the primary photocurrent (Eq. (5)). The total current can be several orders of magnitude greater than the primary photocurrent produced by the photodiode layer. The dependence of the total current on the threshold voltage of a Photo-JFET calculated for a typical device dimension is shown in Fig. 2.

$$I_{Total} = I_D + I_{ph} + I_{o1} \tag{5}$$

Assuming that the voltage threshold is greater than $V_{GS\ Dark}$, the total current produced in the dark condition is equivalent to the reverse saturation current, I_{o1}, of the reverse biased diode (Eq. (6)). In practice, the actual reverse bias leakage current will likely be much higher than the theoretical value and will increase with the reverse bias voltage. However, as shown in Fig. 2(B), the V_{TH} of the Photo-JFET can be carefully engineered to achieve a photocurrent to dark current ratio between 10-10,000 depending upon the required intensity of irradiating light to turn on the JFET channel.

$$I_{TotalDark} = I_{o1} \tag{6}$$

When the illuminating irradiance generates sufficient V_{GS} to exceed V_{TH}, the current versus irradiance curve shifts abruptly from a simple linear current-irradiance relationship, as expected for a photodiode, to a regime where the current level rises several orders of magnitude with increasing irradiance. The dark current level remains flat as long as the V_{GS} in dark is below the ideal minimum threshold V_{TH}. This rapid rise in current results from the phototransistive gain achieved by a Photo-JFET pixel, G_{JFET}, which can be formulated as the ratio of the total current in Eq. 5 to the current from the reverse biased photodiode when illuminated Eq. (7).

$$G_{JFET} = \frac{I_{Total}}{I_{ph} + I_{o1}} \tag{7}$$

When $V_{GS} > V_{TH}$ the gain quickly increases before reaching a peak level after which the gain decreases with increasing irradiance due to the channel current saturation of the JFET (Fig. 2(C)). Although in the JFET saturation regime the gain decreases with increasing irradiance, the total current still increases monotonically with the irradiance in a fashion similar to the natural retinal response, thus extending the dynamic range of the retinal prosthesis.

2.3. Neural stimulation

The total current produced at the Photo-JFET pixel is delivered to retinal tissue through a stimulation electrode in contact with the top of the silicon mesa (Fig. 1(C,D)). For a N-P-N device, anodic stimulation current will be produced by applying positive bias to the top N layer and cathodic stimulation current will be produced by reversing the polarity of bias voltage. Each individual pixel in a retinal prosthesis implant must produce sufficient current to independently stimulate a region of retinal neural cells. The required output current per pixel to reach half-maximal effective stimulation with 10-30μm diameter stimulation electrodes is reported to be between 1.8-7μA based on in vitro studies [20]. Furthermore, the stimulation threshold for individual cells within a single retina may vary due to differences in the morphology and phenotype, as well as the actual distance between stimulating electrodes and target cells over the entire span of an implanted array. Therefore, the total current produced by a Photo-JFET pixel must reach a level of ~10uA for a safe range of NIR irradiance while the V_{TH} of the JFET-channel must be sufficiently high such that the dark current will never inadvertently result in stimulation.

Biomedical Optics EXPRESS

3. Fabrication

The Photo-JFET device structure was realized by microfabrication techniques in a class 100 cleanroom facility. Single pixel test structures for device characterization (Fig. 1B) and array prototypes (Figs. 1(C) and 1(D)) were formed by etching silicon mesas from an epitaxially grown wafer with doped sequential N-P-N layers on a N+ substrate. For in vitro testing, single pixel test structures were interfaced with neural stimulation electrodes fabricated on borosilicate glass discs. This transparent electrode substrate served as the bottom of the recording chamber to allow visualization of retinal neurons with differential interference microscopy for physiological recordings.

3.1. Device fabrication

Pixel mesas were fabricated at 13 µm and 40 µm diameter using a deep reactive ion etching and inductively coupled plasma process to a height of 1.5 µm, to form the back-to-back diode structure. A dielectric layer of SiO_2 was deposited by plasma enhanced chemical vapor deposition over the entire mesa to create a weak inversion layer along the height of the P-Si layer, thereby forming a vertical FET along the mesa sidewall. An opening was etched in the SiO_2 dielectric on top of the silicon mesa and an ITO layer was deposited over it to form a transparent electrical contact. For single pixel test structures, a gold contact pad was deposited on top of the ITO layer off the pixel to allow for probing. A common ground contact shared by each pixel was formed by depositing a gold layer on the back of the device substrate. Pixels in the array prototype were finished with a 10 µm diameter iridium oxide electrode on top of the ITO layer in the space between adjacent mesas.

3.2. Stimulation electrode fabrication

Briefly, electrodes for in vitro retinal stimulation were fabricated by depositing transparent conductive traces of Indium Tin Oxide (ITO) on a borosilicate glass disc. Traces were electrically insulated by a layer of SiNx deposited by plasma enhanced vapor deposition. A hole was etched through the SiNx layer to expose the ITO-electrode contact using reactive ion etching. Iridium oxide electrodes of 30 µm diameter were deposited over each opening by reactive DC sputtering of an Iridium metal target in an Argon (90%) and Oxygen (10%) gas mixture at a thickness of 600 nm. Finally, a layer of Polyethylenedioxythiophene/ Polysulfostyrene (PEDOT/PSS) was deposited on top of the iridium oxide electrode from 0.01 M EDOT in 2.5 g per 100 mL NaPSS (Sigma-Aldrich) by galvanostatic electrodeposition at a fixed current density of 5 mA/cm^2 for 10 seconds in phosphate buffered saline versus an Ag/AgCl electrode. A 400 µm diameter iridium oxide was also fabricated on the periphery of the glass disc to serve as the return electrode.

4. Measured optoelectronic performance of Photo-JFET pixels

The current-voltage characteristics of Photo-JFET pixels were measured under voltage bias and illumination (Fig. 3). Visible light (518nm) and NIR (850nm) were used to investigate device photoresponse. A laser spot of 60µm diameter (full width at half maximum) was projected using a 10x plan infinity corrected long working distance objective (Mitutoyo #46-144) onto all devices so the total power over the spot was adjusted such that each pixel diameter was evaluated under the same irradiance conditions. Measurements of dark current were performed in a darkened environment where irradiance was on the order of $60pW/mm^2$. A source meter (Keysight B2900A) was used to sweep the voltage bias from −2V to 2V at 50mV/s and measure the total current across the silicon mesa.

Both photosensitive regions are sensitive to visible (518nm) and NIR (850nm) light (Fig. 3). The I-V characteristic is slightly asymmetric at equivalent voltage bias of opposite polarity. The bias polarity across the silicon mesa dictates which region of the NPN stack is reverse biased

Biomedical Optics EXPRESS

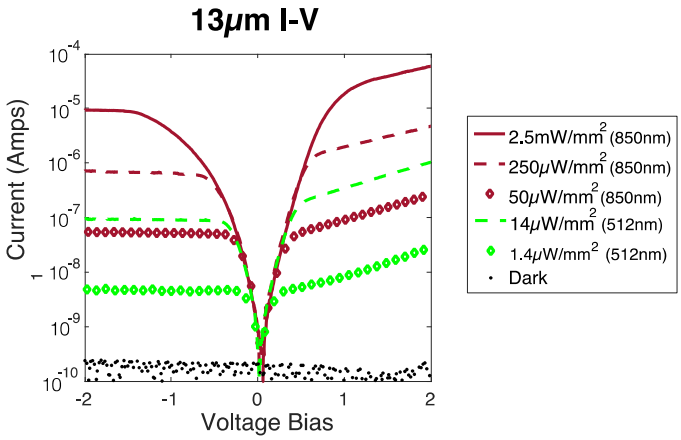

Fig. 3. I-V Characteristics of Photo-JFET pixels for 13 µm diameter pixels under illumination with visible (518 nm) and NIR (850 nm) light.

and thus photosensitive. With positive bias the primary photosensor is the top diode, whereas with negative bias it is the bottom diode. The asymmetry of the photoresponse with voltage bias polarity can be explained by the difference in absorption coefficient of both wavelengths in the top and bottom diodes. Overall, the Photo-JFET pixels have better photoresponse at 518nm than 850nm wavelength light. This difference in photoresponse can be explained by the difference in relative absorption length of the two wavelengths within the 1.5µm height of the silicon mesa, which favors the absorption of shorter wavelength light in the photosensing region of the Photo-JFET. The 40µm pixel devices possess similar I-V characteristics to 13µm pixel devices at equivalent incident light power.

The "turn on" characteristic of the normally-off JFET is dictated by the current output from the primary photo sensing diode that is used to modulate the gate-to-source voltage, V_{GS}, as described above. The Photo-JFET is in the saturation regime with its current modeled by Eq. (3) when $|V_{DS}| > 1V$). At $|V_{DS}|$=1.5V, the dark current for 13µm diameter pixel devices is well below the neural excitation threshold of ~1 µA.

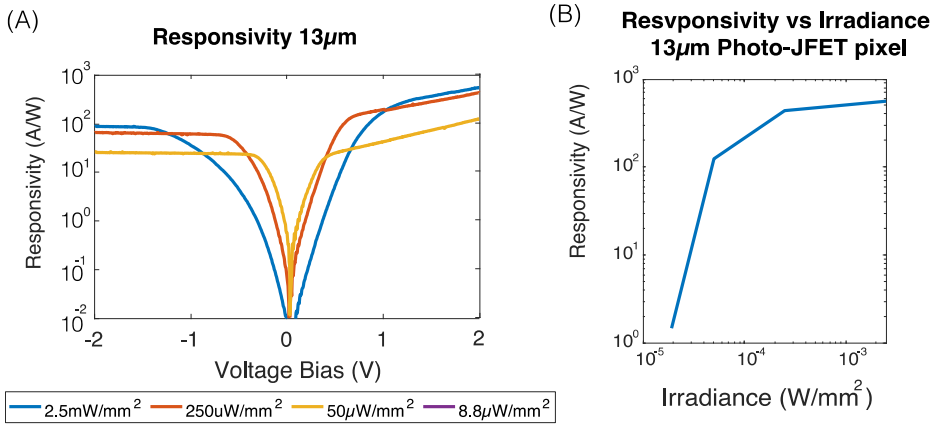

Fig. 4. (A) Voltage dependence of responsivity for NIR illumination (850 nm) of a 13 µm Photo-JFET pixel and (B) Responsivity of a 13 µm diameter pixel vs. NIR irradiance (850 nm) at 2 V bias.

Biomedical Optics EXPRESS

Illumination of the Photo-JFET with 518nm or 850nm light causes the JFET channel to turn on. With sufficient illuminating irradiance, the total current produced by the Photo-JFET pixel is orders of magnitude higher than the primary photocurrent produced by a reverse biased photodiode (Fig. 3). At low irradiance of <10 uW/mm^2, the photoresponsivity is less than 1 A/W, equivalent to a simple photodiode. However, as the light power increases, the effective responsivity rises to 100 A/W with voltage bias (Fig. 4). The required irradiance of 850nm light to turn on the JFET channel is around 50uW/mm^2 for a 13µm pixel and 8uW/mm^2 for a 40µm pixel. Both 13 µm and 40 µm Photo-JFET pixels have similar performance in terms of photoresponsivity. For both devices, we observe that gain reaches the peak value then decreases with increasing irradiance, in agreement with the device model.

5. Utility of Photo-JFET pixels for retinal prosthesis

To investigate how a Photo-JFET pixel can evoke neural stimulation, we devised an ex vivo retinal stimulation strategy. All experimental methods and animal care procedures were approved by the University of California San Diego Institutional Animal Care and Use Committee. Adult rd10 mice (>P60) with photoreceptor cell degeneration were anesthetized with isoflurane and euthanized by decapitation and their retinas were isolated and maintained in Ames medium oxygenated and equilibrated with 95% O_2, 5% CO_2. 2 mm x 2mm retina pieces were transferred to a recording chamber with a glass bottom with the fabricated stimulating electrodes on an upright microscope and perfused with Ames solution (4 ml/min) at 35°C. Retina was placed over stimulating electrodes ganglion cell side up. Retinal ganglion cells (RGCs) were visualized using IR differential interference contrast video microscopy. Recording electrodes were pulled from borosilicate capillary glass to have a final resistance of 4-5 MΩ and filled with Ames medium. Action potentials in RGCs were recorded in the loose patch configuration in voltage clamp mode using a Multiclamp 700b (Molecular Devices). Signals were filtered at 4kHz (4-pole Bessel), digitized at 20 kHz with an ITC-18 (HEKA Electronik) and saved to a PC for offline analysis.

Electrical probes were used to connect the contact pads of the 13µm Photo-JFET test structure to a single 30µm stimulation electrode underneath ganglion cells targeted for recording and a distant 400µm return electrode on the glass disc. An isolated voltage source (Gamry Interface1000E) was used to provide bias across the entire circuit as represented in Fig. 5A. The pixel mesa was illuminated with a 60µm spot of NIR light (850nm) using the method described above at irradiance levels expected to achieve sufficient photocurrent to exceed an expected stimulation threshold of ~1µA based on measured I-V performance. Bias was applied to the circuit for 5ms at + 2V (anodal) followed by 5ms at −2V (cathodal) while the pixel was kept dark or illuminated (360µW/mm^2 or 3.6mW/mm^2). RGC action potentials were observed and counted within the first 40ms following the onset of the stimulus. Each stimulation condition was repeated for 10 consecutive trials separated by 9 seconds and spike counts were averaged for each cell.

Under voltage bias and illumination with NIR light, a single Photo-JFET pixel produced sufficient photocurrent to trigger action potentials in RGCs at both irradiance conditions. The dark current produced at 2V bias elicits negligible spiking activity, on the order of spontaneous firing in RGC. With an average of 5.1 and 6.6 spikes at 360µW/mm^2 and 3.6mW/mm^2 respectively, there are significantly more action potentials for both illumination conditions versus the 0.19 spikes observed in dark ($p < 0.0001$, paired t-test). While more spikes are observed at 3.6mW/mm^2 ($p < 0.005$, paired t-test) the 10x increase in irradiance only corresponds to a 30% increase in elicited action potentials.

Biomedical Optics EXPRESS

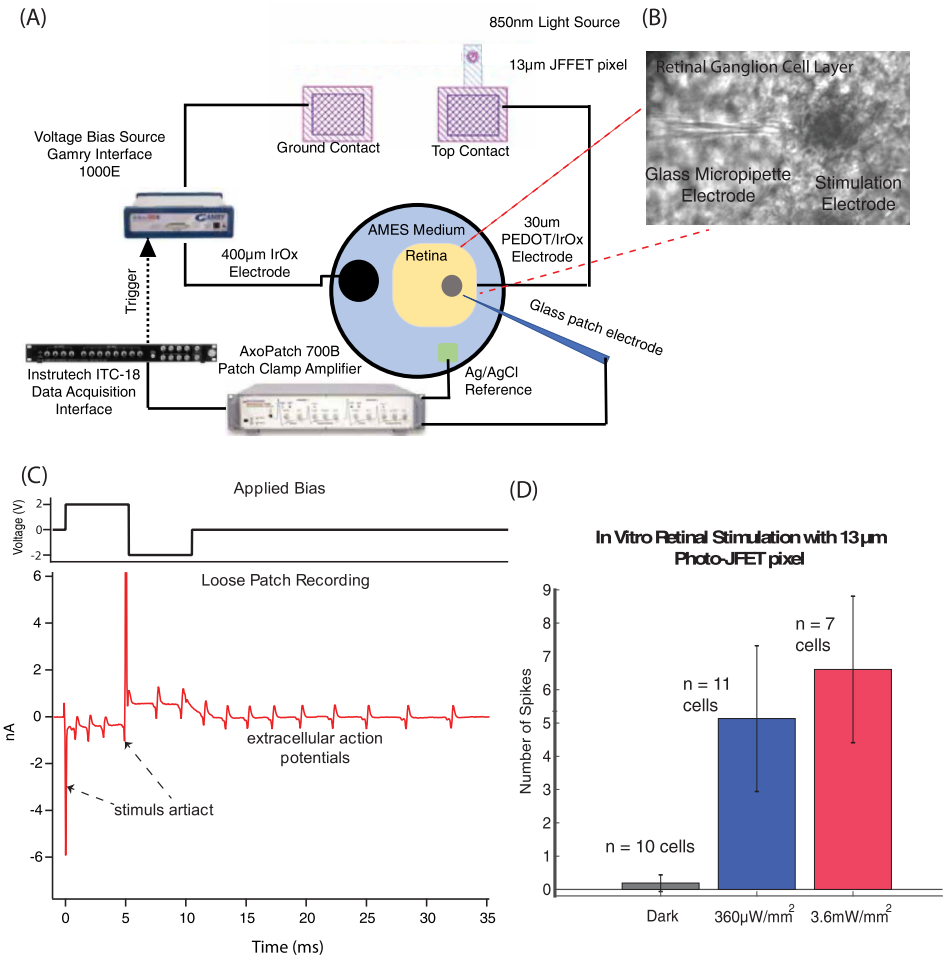

Fig. 5. Overview of the in vitro experiment to demonstrate retinal stimulation with Photo-JFET pixels. (A) diagram of the circuit to connect Photo-JFET pixels on chip to neural stimulation electrodes and the instrumentation used to record stimulated action potentials from retinal neurons (B) 10x microscope image of Rd10 retina atop of PEDOT/IrOx electrode on transparent substrate with a glass micropipette electrode used to loose patch RGC to record action potentials (E) Spiking behavior recorded from RGC in response to electrical stimulation driven by Photo-JFET pixels (D) Comparison of spikes elicited by Photo-JFET stimulation under dark and NIR illumination

6. Discussion

In this work we proposed a novel architecture consisting of a vertical photo junction-field-effect transistor for optoelectronic retinal implants. The Photo-JFET design combines the functions of light sensing and gain that addresses the critical design goal for retinal prosthesis of minimizing pixel size to enable high visual acuity. The design was successfully realized by microfabrication of silicon Photo-JFET pixels of 13µm and 40µm diameter. The device photoresponse was measured under visible and NIR irradiance and demonstrating characteristic JFET gain behavior (Fig. 3). The measured FET photoresponsivity (Fig. 4(B)) corresponded with the calculated theoretical gain behavior for representative pixel size (Fig. 2(C)). The optimal parameters for voltage biasing

Biomedical Optics EXPRESS

and NIR irradiance that produce current in the desired range of >1μA for neural stimulation were identified. We then validated the utility of Photo-JFET pixels for retinal prosthesis with in vitro experiments whereby an optically addressed 13μm pixel successfully stimulated retinal neurons. Therefore, an optically addressed Photo-JFET approach enables use of the smallest reported pixel size for neural stimulation in a retinal prosthesis implant.

While Photo-JFET pixels are responsive to visible light, the irradiance of visible light required (>14μW/mm^2) for sufficient retinal stimulation current is well outside the range of typical retinal irradiance and the safe exposure limit of 518 nm light. Therefore, similar to existing technologies, a NIR source can be used to optically address Photo-JFET array to encode stimulation parameters such as stimulation current and spatial contrast [9,17]. The maximum permissible irradiance of 850 nm on the cornea and lens is 200μW/mm^2 for continuous exposure over 8 hours and 5.9 mW/mm^2 for 5 ms of pulsed exposure at 20 Hz repetition [23,24]. Based on the in vitro proof-of-concept results, a 13 μm pixel can effectively stimulate retinal neural cells within the safety limits of NIR exposure at 360μW/mm^2. Using reported stimulation thresholds as a guideline, Photo-JFET pixels can produce sufficient current for stimulation within a safe range of NIR light at 850 nm (Fig. 6). Alternatively, devices can be optically addressed with less NIR irradiance if the pixel size is expanded. Photo-JFET devices produce similar total output current at equivalent incident light power since the performance is proportional to pixel circumference and primary photocurrent (Eq. 4). At the cost of prosthetic acuity, larger Photo-JFET devices can also produce sufficient current for neural stimulation at much lower NIR irradiance than similarly sized MPDA pixels.

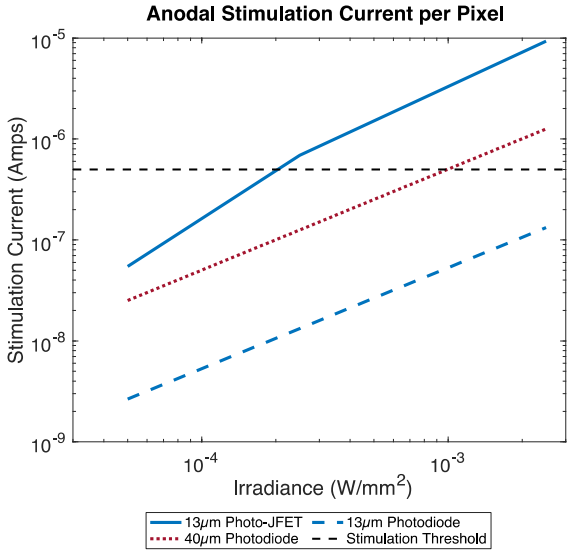

Fig. 6. Comparison of measured current produced by 13 μm Photo-JFET pixels versus theoretical current of passive photodiode pixels at 13 μm and 40 μm diameter under the same illumination conditions with NIR light (850 nm). A responsivity of 0.4 A/W is assumed for passive photodiodes based on reported values [21].

The spatial resolution of a retinal prosthesis is determined by the center-to-center electrode spacing in the array. Specifically, for an implantable MPDA, electrode spacing depends directly on the photosensing area required per individual pixel to produce sufficient current for stimulation. The reported minimum current required to stimulate a retinal neuron in vitro with microelectrodes is ~500 nA for anodic-first stimulation and slightly higher at ~800 nA for cathodic-first at 10 ms pulse duration [25]. A 13 μm Photo-JFET pixel can utilize phototransistive gain to produce enough

Biomedical Optics EXPRESS

current beyond threshold for neural stimulation (Fig. 6). Whereas, a photodiode only approach requires larger pixel of at least 40 µm and NIR light nearing maximum permissible exposure (MPE) to reach stimulation threshold. On this basis, a Photo-JFET pixel-based prosthesis may achieve higher spatial resolution beyond that of existing MPDA technologies.

It is important to consider that while the best theoretical restorable visual acuity is determined by the electrode pitch, electrochemical crosstalk will determine the actual spatial resolution of the array. Crosstalk arises from overlapping signals from adjacent electrodes due to the spread of current density in an ionic environment. Crosstalk can be mitigated by incorporating features such as local return electrodes to focus the electric field at each pixel [26]. Also, a closer apposition of the stimulating electrode to the retinal neural tissue can lower stimulation threshold and help preserve the spatial resolution of a high-density array [27,28]. Given the simplicity of the device structure and miniature size of the pixel, a Photo-JFET array can be modified to integrate features such as local return electrodes or 3-D structures to mitigate the effect of crosstalk in future iterations. For example, the silicon mesa comprising the Photo-JFET pixel can be etched from the epitaxial silicon substrate to form a micropillar with a vertical height on the order of 10-50 µm.

In the United States the criteria for legal blindness is visual acuity worse than 20/200 or a visual field less than 20°. A clinically meaningful retinal prosthesis for AMD patients must restore high acuity central vision on the order of 20/100 or better to enable reading or large font. Previous studies of MPDA devices have demonstrated successful retinal neural stimulation in clinical experiments. However, the measured prosthetic visual acuity in human patients was typically quite low, below 20/540 [13,14]. The Photo-JFET approach we described allows for the smallest reported pixel size used for an optoelectronic retinal prosthesis by vertically integrating a gain mechanism within the body of the photosensor. We contemplate an implantable version of the Photo-JFET prosthesis will consist of an array of pixels on silicon die attached to a flexible polymer substrate, connected via an inductive link to an external power source to supply the voltage bias. Photo-JFET pixels of 13 µm diameter can be arrayed at a dense pitch, which may offer a substantial improvement in clinical visual acuity for patients with degenerative retinal disease.

7. Conclusions

We developed a novel vertical junction-field-effect transistor architecture that achieves photosensing, gain, and neural stimulation in a compact pixel size for high visual acuity retinal prosthesis. The design was realized by a vertically integrated back-to-back diode structure in parallel with a sidewall FET. Photo-JFET pixels were successfully fabricated at pixel dimensions approaching cellular scale. A simple bias mechanism and optical addressing using NIR light produce a broad range current for neural stimulation per pixel. We demonstrated in a proof-of-concept experiment that a single Photo-JFET pixel can effectively stimulate retinal neurons in an in vitro model of degenerative retinal disease. The Photo-JFET design allows for smaller pixel sizes with improved functionality versus passive microphotodiode arrays. This work demonstrates an important development towards high visual acuity retinal prostheses that may help restore clinically meaningful vision, better than 20/100 in patients with degenerative retinal disease.

Funding

National Science Foundation (ECCS-1542148); National Institutes of Health (EY029259).

Disclosures

SD: Nanovision Biosciences, Inc. (F,P); YLiu: Nanovision Biosciences, Inc. (E), NOW: Nanovision Biosciences, Inc. (F,C,P, R) YLo: Nanovision Biosciences, Inc. (F, C, P,R)

Biomedical Optics EXPRESS

References

1. D. T. Hartong, E. L. Berson, and T. P. Dryja, "Retinitis pigmentosa Prevalence and inheritance patterns," Lancet **368**(9549), 1795–1809 (2006).
2. S. P. Daiger, S. J. Bowne, and L. S. Sullivan, "Perspective on genes and mutations causing retinitis pigmentosa," Arch. Ophthalmol. **125**(2), 151–158 (2007).17296890
3. W. L. Wong, X. Su, X. Li, C. M. G. Cheung, R. Klein, C. Y. Cheng, and T. Y. Wong, "Global prevalence of age-related macular degeneration and disease burden projection for 2020 and 2040: A systematic review and meta-analysis," Lancet Glob. Heal. **2**(2), 106–116 (2014).
4. K. L. Pennington and M. M. DeAngelis, "Epidemiology of age-related macular degeneration (AMD): associations with cardiovascular disease phenotypes and lipid factors," Eye Vis. **3**(1), 34 (2016).
5. G. A. Goetz and D. V. Palanker, "Electronic approaches to restoration of sight," Rep. Prog. Phys. **79**(9), 096701 (2016).
6. J. D. Weiland and M. S. Humayun, "Retinal prosthesis," IEEE Trans. Biomed. Eng. **61**(5), 1412–1424 (2014).
7. L. da Cruz, J. D. Dorn, M. S. Humayun, G. Dagnelie, J. Handa, P. O. Barale, J. A. Sahel, P. E. Stanga, F. Hafezi, A. B. Safran, J. Salzmann, A. Santos, D. Birch, R. Spencer, A. V. Cideciyan, E. de Juan, J. L. Duncan, D. Eliott, A. Fawzi, L. C. Olmos de Koo, A. C. Ho, G. Brown, J. Haller, C. Regillo, L. V. Del Priore, A. Arditi, and R. J. Greenberg, "Five-Year Safety and Performance Results from the Argus II Retinal Prosthesis System Clinical Trial," Ophthalmology **123**(10), 2248–2254 (2016).
8. M. S. Humayun, J. D. Dorn, L. Da Cruz, G. Dagnelie, J. A. Sahel, P. E. Stanga, A. V. Cideciyan, J. L. Duncan, D. Eliott, E. Filley, A. C. Ho, A. Santos, A. B. Safran, A. Arditi, L. V. Del Priore, and R. J. Greenberg, "Interim results from the international trial of second sight's visual prosthesis," Ophthalmology (**119**(4), 779–788 (2012).22244176
9. D. Palanker, A. Vankov, P. Huie, and S. Baccus, "Design of a high-resolution optoelectronic retinal prosthesis," J. Neural Eng. **2**(1), S105–S120 (2005).
10. Y. T. Yang, P. K. Lin, C. Wan, W. C. Yang, L. J. Lin, C. Y. Wu, and C. C. Chiao, "Responses of rabbit retinal ganglion cells to subretinal electrical stimulation using a silicon-based microphotodiode array," Invest. Ophthalmol. Visual Sci. **52**(13), 9353–9361 (2011).
11. K. Stingl, K. U. Bartz-Schmidt, D. Besch, A. Braun, A. Bruckmann, F. Gekeler, U. Greppmaier, S. Hipp, G. Hortdorfer, C. Kernstock, A. Koitschev, A. Kusnyerik, H. Sachs, A. Schatz, K. T. Stingl, T. Peters, B. Wilhelm, and E. Zrenner, "Artificial vision with wirelessly powered subretinal electronic implant alpha-IMS," Proc. R. Soc. B Biol. Sci. **280**(1757), 20130077 (2013).23427175
12. C. L. Lee and C. C. Hsieh, "A 0.8-V 4096-pixel CMOS sense-and-stimulus imager for retinal prosthesis," *IEEE Trans. Electron Devices* (2013).
13. K. Stingl, K. U. Bartz-Schmidt, D. Besch, C. K. Chee, C. L. Cottriall, F. Gekeler, M. Groppe, T. L. Jackson, R. E. MacLaren, A. Koitschev, A. Kusnyerik, J. Neffendorf, J. Nemeth, M. A. N. Naeem, T. Peters, J. D. Ramsden, H. Sachs, A. Simpson, M. S. Singh, B. Wilhelm, D. Wong, and E. Zrenner, "Subretinal Visual Implant Alpha IMS - Clinical trial interim report," Vision Res. **111**, 149–160 (2015).
14. T. L. Edwards, C. L. Cottriall, K. Xue, M. P. Simunovic, J. D. Ramsden, E. Zrenner, and R. E. MacLaren, "Assessment of the Electronic Retinal Implant Alpha AMS in Restoring Vision to Blind Patients with End-Stage Retinitis Pigmentosa," Ophthalmology **125**(3), 432–443 (2018).
15. R. Daschner, U. Greppmaier, M. Kokelmann, S. Rudorf, R. Rudorf, S. Schleehauf, and W. G. Wrobel, "Laboratory and clinical reliability of conformally coated subretinal implants," Biomed. Microdevices **19**(1), 7–8 (2017).
16. D. Boinagrov, X. Lei, G. Goetz, T. I. Kamins, K. Mathieson, L. Galambos, J. S. Harris, and D. Palanker, "Photovoltaic Pixels for Neural Stimulation: Circuit Models and Performance," IEEE Trans. Biomed. Circuits Syst. **10**(1), 85–97 (2016).
17. S. Ha, M. L. Khraiche, A. Akinin, Y. Jing, S. Damle, Y. Kuang, S. Bauchner, Y.-H. Lo, W. R. Freeman, G. A. Silva, and G. Cauwenberghs, "Towards high-resolution retinal prostheses with direct optical addressing and inductive telemetry," J. Neural Eng. **13**(5), 056008 (2016).
18. B. Bosse, S. Damle, A. Akinin, Y. Jing, D. U. Bartsch, L. Cheng, N. Oesch, Y. H. Lo, G. Cauwenberghs, and W. R. Freeman, "In vivo photovoltaic performance of a silicon nanowire photodiode–based retinal prosthesis," Investig. Ophthalmol. Vis. Sci. **59**(15), 5885–5892 (2018).30550611
19. H. Lorach, G. Goetz, R. Smith, X. Lei, Y. Mandel, T. Kamins, K. Mathieson, P. Huie, J. Harris, A. Sher, and D. Palanker, "Photovoltaic restoration of sight with high visual acuity," Nat. Med. **21**(5), 476–482 (2015).
20. A. Corna, T. Herrmann, and G. Zeck, "Electrode-size dependent thresholds in subretinal neuroprosthetic stimulation," J. Neural Eng. **15**(4), 045003 (2018).
21. J. D. Loudin, D. M. Simanovskii, K. Vijayraghavan, C. K. Sramek, A. F. Butterwick, P. Huie, G. Y. McLean, and D. V. Palanker, "Optoelectronic retinal prosthesis: system design and performance," J. Neural Eng. **4**(1), S72–S84 (2007).
22. H. Lorach, J. Wang, D. Y. Lee, R. Dalal, P. Huie, and D. Palanker, "Retinal safety of near infrared radiation in photovoltaic restoration of sight," Biomed. Opt. Express **7**(1), 13–21 (2016).
23. D. Sliney, D. Aron-Rosa, F. DeLori, F. Fankhauser, R. Landry, M. Mainster, J. Marshall, B. Rassow, B. Stuck, S. Trokel, T. M. West, and M. Wolffe, "Adjustment of guidelines for exposure of the eye to optical radiation from ocular instruments: statement from a task group of the International Commission on Non-Ionizing Radiation Protection (ICNIRP)," Appl. Opt. **44**(11), 2162–2176 (2005).
24. ANSI, *American National Standard for Safe Use of Lasers* (2014), **ANSI Z136.**

Biomedical Optics EXPRESS

25. D. Boinagrov, S. Pangratz-Fuehrer, G. Goetz, and D. Palanker, "Selectivity of direct and network-mediated stimulation of the retinal ganglion cells with epi-, sub- and intraretinal electrodes," J. Neural Eng. **11**(2), 026008 (2014).
26. T. Flores, G. Goetz, X. Lei, and D. Palanker, "Optimization of return electrodes in neurostimulating arrays," J. Neural Eng. **13**(3), 036010 (2016).
27. T. Flores, X. Lei, T. Huang, H. Lorach, R. Dalal, L. Galambos, T. Kamins, K. Mathieson, and D. Palanker, "Optimization of pillar electrodes in subretinal prosthesis for enhanced proximity to target neurons," J. Neural Eng. **15**(3), 036011 (2018).
28. K. Ganesan, A. Stacey, H. Meffin, S. Lichter, U. Greferath, E. L. Fletcher, and S. Prawer, "Diamond penetrating electrode array for Epi-Retinal prosthesis," *2010 Annu. Int. Conf. IEEE Eng. Med. Biol. Soc. EMBC'10 (March)*, 6757–6760 (2010).